Research Square

Preprints are preliminary reports that have not undergone peer review.
They should not be considered conclusive, used to inform clinical practice,
or referenced by the media as validated information.

Research on multi-component sodium silicate coated sand with both moisture resistance and collapsibility

Tengxiao Luo
Polymer Research Institute of Sichuan University
Junhua Zhang
zhangjh@scu.edu.cn

Polymer Research Institute of Sichuan University

Research Article

Keywords: coated sand, sodium silicate, moisture resistance, collapsibility

Posted Date: October 1st, 2026

DOI: https://doi.org/10.21203/rs.3.rs-10725468/v1

License: This work is licensed under a Creative Commons Attribution 4.0 International License.
Read Full License

Additional Declarations: No competing interests reported.

Abstract

Sodium silicate offers an eco-friendly alternative to organic binder system like phenolic resin coated sand, which can be limited by toxic emissions during thermal processing. However, its poor moisture resistance and collapsibility binders have impeded their widespread industrial adoption. This study introduced hydroxyethyl cellulose (HEC) to improve collapsibility, tung oil (TO) to enhance moisture resistance via carboxyl-silicate reactions, and silane coupling agent KH550 to bridge organic and inorganic components. Moisture resistance was evaluated by comparing initial and 24-hour strength, while collapsibility was quantified as the mass ratio of sand passing through a 10-mesh sieve after high-temperature treatment. Single-factor and orthogonal L9(3^3) experiments were conducted to investigate the effects of HEC, TO, and KH550 on strength, moisture resistance, and collapsibility. Maximum initial tensile strength (1.66 MPa) was achieved at HEC 3%, TO 2%, KH550 10%. Under 65% RH, HEC 5%, TO 2%, KH550 5% yielded optimal 24-hour residual strength (0.68 MPa) and collapsibility (47.16%); under 50% RH, HEC 4%, TO 2%, KH550 15% achieved 1.10 MPa with 70.06% retention and 72.69% collapsibility. SEM confirmed intact bonding bridges after 24-hour storage. These findings provide a rational design strategy for tailoring modified sodium silicate binders to specific service environments.

1. Introduction

The current landscape of sodium silicate coated sand technology is being reshaped by the escalating environmental regulations and the foundry industry's imperative to mitigate hazardous emissions associated with organic resin binders. Conventional organic binder systems such as phenolic urethane and furan resins—release substantial quantities of volatile organic compounds (VOCs), including benzene, toluene, and formaldehyde, during core-making, curing, and casting processes, posing significant risks to both ecological sustainability and occupational health[1, 2]. In response, inorganic silicate-based systems, particularly sodium silicate coated sands, have garnered renewed attention as a promising alternative capable of delivering high dimensional accuracy and mechanical performance while virtually eliminating toxic gas evolution[3, 4]. Silicate coated sands and cores are increasingly employed in high-volume production of critical castings, where their low loss-on-ignition and favorable gas evolution profiles reduce casting defects such as porosity, veining, and metal penetration[5].

Among the prevailing hardening routes, the CO_2-gassing process offers the advantages of simple equipment, low cost, and rapid curing, and recent studies have further improved its strength through modified sodium silicate and composite strength enhancers. However, it remains intrinsically limited by the over-gassing phenomenon, in which excess CO_2 reacts with NaOH to form flaky $NaHCO_3$ crystals that fracture the binder film and progressively degrade core strength[6–8]. In addition to the CO_2-gassing route, the self-hardening process, in which organic ester hardeners are blended into the sand mixture, allows irreversible curing at room temperature without any external heating or gas supply, offering low energy consumption and flexible control of working and stripping times, typically at modest binder levels of 2–3%; it is therefore particularly suitable for medium- and large-sized molds in jobbing foundries,

although chemically cured self-hardening sands exhibit weak initial strengths, unsatisfactory collapsibility, and sluggish curing at low ambient temperatures[9, 10].

Core box processes, particularly the low-temperature warm core box combined with ambient-temperature gas blowing, provide high dimensional accuracy, excellent surface quality, and significant energy savings, yet cores hardened solely by physical gelation within the box are prone to non-uniform curing, low bond strength, and rapid strength degradation under humid storage[11–13]. Notably, when sodium silicate is employed in the coated sand form and cured by thermal hardening, the process combines the merits of both worlds: the dry, free-flowing coated granules ensure excellent filling of complex core cavities, while heating consolidates the binder film without any risk of over-blowing. Owing to these advantages, together with the modest retrofitting requirements of existing hot-box equipment, thermal hardening remains the process of choice in some foundries. Nevertheless, thermally hardened sodium silicate coated sands are confronted with two persistent drawbacks that have impeded their wider application[14, 15]. On the one hand, the hydrophilic silicate gel continuously absorbs atmospheric moisture during storage, hydrolyzing the Si–O–Si bonding bridges and causing a pronounced loss of strength; on the other hand, the ceramic-like silicate network retains high residual strength after casting, so that the cores resist disintegration and demand laborious mechanical removal, which increases cleaning costs and risks damaging the casting surfaces.

Although various modification strategies—such as inorganic composite additives, micro-silica, and hot-air-assisted curing—have been explored to enhance the moisture resistance of silicate-bonded sands, most existing formulations are directed toward a single performance target, and few have addressed the moisture–collapsibility trade-off in a synergistic manner; in fact, measures that densify the network to resist moisture often aggravate the post-casting shakeout problem. To bridge this gap, the present work develops a multi-component modification strategy for thermally hardened sodium silicate coated sand, in which HEC is introduced to improve collapsibility through thermally induced decomposition and pore formation, TO is introduced to enhance moisture resistance via carboxyl–silicate reactions, and the silane coupling agent KH550 is employed to bridge the organic and inorganic phases. Single-factor and orthogonal L9(3^3) experiments were conducted to optimize the formulation, with the initial and 24-hour residual tensile strengths, strength retention rates, and collapsibility systematically evaluated under two humidity levels (50% and 65% RH). By establishing environment-dependent optimal formulations, this work opens up a promising avenue for reconciling the environmental friendliness of inorganic binders with the stringent performance requirements of modern foundry practice.

2. Experiment section

2.1. Materials

The raw sand with a mesh size of 100 mesh used in the experiment was purchased from Dalin Mould Sand Co., Ltd., Tongliao, China. Sodium silicate powder was supplied by Sichuan Jianyizhixing Ceramics

Co., Ltd. HEC was obtained from Hubei Chenghai Chemical Co., Ltd. Silane coupling agent KH550 and TO were provided by Chengdu Dingsheng Times Technology Co., Ltd.

2.2. Experimental methods

2.2.1. Preparation of sodium silicate solution

Sodium silicate powder and deionized water were mixed at a mass ratio of 2:3 and stirred thoroughly at room temperature to prepare a sodium silicate solution with a solid content of approximately 40%. The prepared solution was stored in a cool and sealed place for subsequent use.

2.2.2. Preparation of modified sodium silicate-coated sand specimens

First, the raw sand was dried at 70 °C for 0.5 h to remove the residual moisture as completely as possible and then cooled to ambient temperature. The HEC was thoroughly mixed with the sodium silicate solution, and the resulting binder system was subsequently added to the sand and vigorously stirred in a sand mixer for 120 s. KH550 was then introduced, and the mixture was continuously stirred for another 120 s. Finally, TO was added, and the blend was stirred for an additional 120 s to obtain a sodium silicate-coated sand. The sodium silicate-coated sand was rapidly filled into a dog-bone mould and compacted as densely as possible, with the surface of the sand specimen levelled as evenly as feasible. The mould was subsequently maintained at 160 °C for 0.5 h, after which it was removed and demoulded to yield the final sand specimen. The simplified process flow diagram is shown in Fig. 1.

2.2.3. Single-factor analysis and orthogonal experimental design

HEC, KH550, and TO each exert distinct influences on the tensile strength, moisture resistance, and collapsibility of the sodium silicate-coated sand. To determine the optimal dosage of each component, a single-factor analysis was first conducted by systematically varying the addition level of each additive individually, with the retained tensile strength of the sand specimen after 24 h serving as the evaluation criterion. Nine gradient levels were established for each modifier: 1%, 2%, 3%, 4%, 5%, 7.5%, 10%, 12.5%, and 15% (all relative to the mass of sodium silicate). During these experiments, the following parameters were held constant: reaction temperature at 160℃, sodium silicate dosage at 1.5 wt% of the raw sand, and reaction time at 0.5 h. All other factors remained unchanged while varying only the target modifier dosage.

Building upon the single-factor experimental results, a three-factor three-level orthogonal experiment was designed to further investigate the combined effects of HEC, KH550, and TO dosages on the 24-hour residual tensile strength of the modified sodium silicate-coated sand. The orthogonal array L9(3^3) was selected, and the factor levels were determined based on the optimal ranges identified from the preceding single-factor analyses. Range analysis was performed on the orthogonal experimental data to establish the optimal combination of factors. Finally, confirmatory tests were carried out to validate the optimal formulation identified from the orthogonal experiment, thereby ensuring the reliability and reproducibility of the results. Six replicate tests were conducted for each experimental run, and the

average of the six measurements was reported as the result. The orthogonal experimental design matrix is presented in Table 1.

Table 1 Orthogonal Experiment Table L9(3^3)

Factor	A (HEC, wt% of sodium silicate)	B (TO, wt% of sodium silicate)	C (KH550, wt% of sodium silicate)
Level 1	3	1	5
Level 2	4	2	10
Level 3	5	5	15

2.2.4. Test of sample characterization

The tensile strength of the samples with storage time of <1 min and 24 h was measured using an SWY hydraulic strength testing machine. The samples stored for 24 h were calcined in a muffle furnace at 400 °C for 5 minutes and then taken out. The calcined sand samples were sieved using a SYS-21J vibrating sieve equipped with a 10-mesh screen, operating at a vibration frequency of 50 rpm for 5 min. The sand retained on the sieve and the sand passing through the sieve were collected and weighed separately, and the mass ratio of the sieved samples to the unsieved samples was calculated as the characterization index of the sample collapsibility. The moisture resistance of the samples was characterized by the tensile strength retention rate after storage at 25 °C and 50% or 65% relative humidity for 24 h.

The surface morphology and composition of the bonding bridges at the fracture surface of the samples were observed using a QUANTA-200 scanning electron microscope (SEM) and an energy dispersive spectrometer (EDS).

Fourier transform infrared (FTIR) spectroscopy analysis was performed on the unmodified and modified sodium silicate adhesive systems using a Nicolet Protégé 460 Fourier transform infrared spectrometer, operating in transmission mode with an average of 32 scans in the range of 400-4000 cm^{-1}.

3. Result and discussion

3.1 The FTIR Spectra of Different Sodium Silicate Systems

Figure 2 presents the FTIR spectra of unmodified sodium silicate, modified sodium silicate, and thermally treated modified sodium silicate systems. The unmodified sodium silicate at 25 ℃, represented by the black curve, exhibits characteristic absorption bands at approximately 3439 cm^{-1}, 1651 cm^{-1}, 1407 cm^{-1}, 1013 cm^{-1}, and 891 cm^{-1}. These bands correspond to O–H stretching, H–O–H bending of adsorbed water, Si–O–Na bending, Si–O–Si asymmetric stretching, and Si–O–Si symmetric

stretching and bending vibrations, respectively. The Si–O–Si stretching band position in sodium silicate is directly correlated with the polymerization degree of silicate anions, where lower wavenumbers near ~1000-1020 cm^{-1} correspond to chain-like Q^2 species, while higher wavenumbers near ~1080-1100 cm^{-1} indicate three-dimensional Q^3 and Q^4 network structures [26, 27]. The predominance of the single broad band at 1013 cm^{-1} in the unmodified system suggests a loosely cross-linked silicate network dominated by Q^2 and Q^3 species with limited connectivity [28].

Upon modification with HEC, KH550, and TO at 25 ℃, the system represented by the red curve exhibits significant spectral evolution. The emergence of absorption bands at 2961 and 2907 cm^{-1}, attributed to the asymmetric and symmetric stretching vibrations of $–CH_2–$ and $–CH_3$ groups from KH550 alkyl chains, confirms the successful incorporation of organosilane moieties into the inorganic matrix. KH550 undergoes hydrolysis of its ethoxy groups followed by condensation with surface hydroxyl groups to form stable Si–O–Si covalent bonds, establishing a molecular bridge between organic and inorganic phases [29, 30]. More notably, the Si–O–Si asymmetric stretching band at 1013 cm^{-1} undergoes a pronounced blue shift and splits into doublets at 1097 and 1025 cm^{-1}, accompanied by the emergence of a distinct band at 802 cm^{-1}. This spectral transformation indicates a substantial increase in the degree of polymerization of the silicate network, whereby the hydrolyzed silanol groups of KH550 condense with the silicate oligomers to form additional Si–O–Si bridges, thereby promoting the transition from Q^2 to Q^3 and Q^4 structures. The concurrent narrowing of the O–H stretching band and the slight red shift of the H–O–H bending mode from 1651 to 1646 cm^{-1} suggest a reorganization of the hydrogen-bonding network and a partial displacement of physically adsorbed water molecules by the organic modifiers.

Following thermal treatment at 160 ℃, the system represented by the blue curve retains the organic signatures at 2963, 2924, and 2850 cm^{-1} with enhanced definition. This retention implies that the thermal protocol does not induce degradation of the organic constituents but rather facilitates their ordered arrangement within the inorganic framework. The Si–O–Si asymmetric stretching doublets at 1097 and 1025 cm^{-1} persist with an increased intensity ratio, and the low-wavenumber modes at 866 and 802 cm^{-1} become more pronounced, collectively evidencing thermally activated condensation reactions that further densify the siloxane network cross-linking density. The blue shift of the H–O–H bending vibration to 1631 cm^{-1} reflects a reduction in physiosorbed water content because of thermal dehydration. The appearance of a weak yet discernible band at 1262 cm^{-1} may be tentatively assigned to Si–C stretching or C–O–C ether linkage vibrations from the HEC component, suggesting the establishment of a stable organic–inorganic hybrid architecture.

After storage under ambient conditions at 25 ℃ and 60% relative humidity for one day, the system represented by the green curve exhibits a considerably broadened O–H stretching band near 3435 cm^{-1}, while the H–O–H bending mode remains essentially unchanged at 1630 cm^{-1}. These spectral changes indicate reversible moisture uptake from the humid atmosphere. Despite this hygroscopic behavior, the characteristic Si-O-Si framework vibrations at 1097, 1025, 866, and 802 cm^{-1} are preserved without

significant shift or degradation, demonstrating the structural integrity and hydrolytic stability of the thermally cured hybrid network. The emergence of additional bands at 1458 and 1262 cm^{-1}, coupled with subtle perturbations in the C–H stretching region, suggests that adsorbed water molecules interact with the organic functionalities, inducing localized conformational adjustments without compromising the overall network connectivity.

In summary, the multi-component modification strategy synergistically enhances the structural organization of the sodium silicate binder: KH550 serves as a molecular bridge via Si–O–Si covalent linkages, tethering the organic modifiers to the inorganic silica sand substrate, while concurrently imparting hydrophobic shielding through its alkyl chains to elevate the overall moisture resistance of the system. The carboxyl groups present in TO, which contain long-chain fatty acids, react with the hydroxyl groups in the sodium silicate matrix, thereby reinforcing the hydrolytic stability of the binder network. HEC was selected as the additive owing to its exceptional dispersibility in strongly alkaline sodium silicate solutions—a critical advantage over conventional polymers that precipitate upon incorporation into such high-pH environments—ensuring uniform distribution throughout the binder matrix and, upon thermal calcination at elevated temperatures, complete decomposition to generate porous channels that substantially enhance the collapsibility of the coated sand. Furthermore, the incorporation of TO and KH550 as organic modifiers contributes additional combustible fractions that facilitate the thermal disintegration of the ceramic bonding phase, thereby collectively improving the post-casting shakeout performance.

3.2. The micro-morphology of unmodified and modified sodium silicate-coated sand

Fig. 3 presents the SEM micrographs and corresponding EDS spectra of sodium silicate-coated sand samples with and without organic modification. As shown in Fig. 3(a), the modified sample (containing a small amount of HEC, TO, and KH560) exhibits a relatively smooth surface morphology with intact spherical particles and is partially connected by bonding bridges formed by the modified sodium silicate binder, indicating uniform coating coverage. The EDS analysis (Fig. 3(b)) reveals the presence of C (37.48 at%), O (48.75 at%), Na (2.61 at%), and Si (10.22 at%), confirming the coexistence of the inorganic sodium silicate binder and the introduced organic modifiers. In contrast, the unmodified sodium silicate-coated sand (Fig. 3(c)) displays a rougher surface with visible defects, including several holes (marked by red circles), which are attributed to the inherent brittleness and poor film-forming ability of pure sodium silicate. The corresponding EDS spectrum (Fig. 3(d)) shows a similar elemental composition, suggesting that the surface chemistry is dominated by the sodium silicate binder itself.

After storage at 25 °C and 60% RH for 24 h, the modified sample (Fig. 3(e)) retains relatively intact bonding bridges (highlighted by blue squares) with minimal structural degradation, demonstrating that the organic modification significantly enhances the moisture resistance of the sodium silicate binder. This structural preservation is directly correlated with the maintained mechanical strength of the modified sample under humid conditions.

In sharp contrast, the unmodified sample (Fig. 3(f)) exhibits severe structural deterioration after the same aging treatment, characterized by extensive cracking, void formation, and complete disruption of the bonding bridges. These defects are ascribed to the poor moisture resistance of pure sodium silicate, which undergoes substantial hydration-induced swelling and structural collapse upon exposure to humid environments. Consequently, the unmodified sodium silicate-coated sand suffers from drastic strength reduction. These comparative results collectively demonstrate that the incorporation of HEC, TO, and KH550 effectively suppresses moisture-induced deterioration, thereby preserving the structural integrity and bonding performance of sodium silicate-coated sand systems under ambient humid conditions.

3.3. The tensile strengths of sodium silicate systems

The individual effects of KH550, TO, and HEC on the tensile strength of the sodium silicate-coated sand were systematically investigated as a function of additive content, with the results presented in Fig. 4.

For KH550, the tensile strength initially decreased from 0.37 MPa at 0 wt% to a minimum of 0.19 MPa at 2 wt%, followed by a gradual increase with further addition, reaching a maximum of 0.59 MPa at 15 wt%. For TO, the tensile strength displayed a non-monotonic variation, peaking at 0.57 MPa at 5 wt% before declining sharply to 0.26 MPa at 7.5 wt%. In the case of HEC, the tensile strength increased to a peak of 0.52 MPa at 5 wt%, followed by a gradual decline with further increasing content.

These results indicate that each additive exerts a distinct concentration-dependent effect on the tensile strength, and the optimal dosage ranges differ significantly among the three modifiers. Based on the single-factor experimental results, a three-factor three-level orthogonal experiment was designed and conducted using the orthogonal array L9(3^3) to investigate the combined effects of HEC, TO, and KH550 dosages on the tensile strength and strength retention rate of modified sodium silicate-coated sand. The factor levels were selected according to the optimal ranges identified from the preceding single-factor analyses, as summarized in Table 1, and the obtained experimental data are presented in Table 2 and Fig. 5. The range analysis was performed to evaluate the influence of each factor on the initial tensile strength, the 24-hour residual tensile strength, and the strength retention rate. The mean values (k_1, k_2, k_3) for each factor at three levels and the corresponding ranges (R) are summarized in Table 3.

Table 2 Orthogonal Test Results for Tensile Strength

Run	Factor A (HEC, wt%)	Factor B (TO, wt%)	Factor C (KH550, wt%)	Tensile strength < 1 min (MPa)	Tensile strength at 24 h, 65% RH (MPa)	Tensile strength at 24 h, 50% RH (MPa)
1	1(3)	1(1)	1(5)	1.61	0.62	0.76
2	1(3)	2(2)	2(10)	1.66	0.60	0.88
3	1(3)	3(5)	3(15)	1.63	0.62	0.73
4	2(4)	1(1)	2(10)	1.53	0.47	1.04
5	2(4)	2(2)	3(15)	1.57	0.54	1.10
6	2(4)	3(5)	1(5)	1.36	0.57	0.95
7	3(5)	1(1)	3(15)	1.38	0.67	0.89
8	3(5)	2(2)	1(5)	1.44	0.68	0.86
9	3(5)	3(5)	2(10)	1.54	0.61	0.83

Table 3 Analysis of orthogonal experimental results for tensile strength

Response	Factor	k_1	k2	k3	R	Rank
Tensile strength < 1 min (MPa)	A(HEC)	1.63	1.49	1.45	0.18	1
	B(TO)	1.51	1.56	1.51	0.04	3
	C(KH550)	1.47	1.58	1.53	0.11	2
Tensile strength at 24 h, 65%RH (MPa)	A (HEC)	0.61	0.53	0.65	0.12	1
	B(TO)	0.59	0.61	0.60	0.01	3
	C(KH550)	0.62	0.56	0.61	0.06	2
Tensile strength at 24 h, 50% RH (MPa)	A (HEC)	0.79	1.03	0.86	0.24	1
	B(TO)	0.90	0.95	0.84	0.11	2
	C(KH550)	0.86	0.92	0.91	0.06	3

The range analysis reveals distinct influence hierarchies across the three responses, with notable consistency in the optimal factor levels. For the initial tensile strength measured within 1 min, HEC dosage exerts the most pronounced influence (R = 0.180 MPa), followed by KH550 (R = 0.107 MPa) and TO (R = 0.050 MPa). The theoretically optimal combination predicted by the mean value analysis is $A_1B_2C_2$, with a calculated theoretical maximum of 1.663 MPa. Remarkably, the actual maximum initial strength of 1.66 MPa is achieved by Run 2, demonstrating exact concordance between the theoretical

prediction and experimental observation. This validates the reliability of the orthogonal experimental design for identifying optimal formulations in the initial strength regime.

For the 24-hour residual tensile strength at 65% RH, HEC dosage remains the primary determinant, followed by KH550 and TO. The theoretically optimal combination is $A_3B_2C_1$, with a theoretical maximum of 0.689 MPa. The actual maximum of 0.68 MPa is achieved by Run 8, again demonstrating exact concordance. The dominance of HEC at the highest level under high-humidity conditions underscores the critical role of the cellulose either film-forming function in providing sustained physical protection against aggressive moisture attack.

For the 24-hour residual tensile strength at 50% RH, HEC dosage again dominates, followed by TO and KH550. The theoretically optimal combination is $A_2B_2C_2$ (HEC = 4%, TO = 2%, KH550 = 10%). However, the actual maximum of 1.10 MPa is achieved by Run 5 ($A_2B_2C_3$: HEC = 4%, TO = 2%, KH550 = 15%). Based on the primary orthogonal experimental results, the deviation between the theoretically optimal formulation and the actual maximum for the 24-hour residual tensile strength at 50% RH warrants targeted comparative analysis. Six replicate tests were conducted for each experimental run, and the average of the six measurements was reported as the result. The results of the validation experiments are presented in Table 4.

Table 4 Validation test for tensile strength

Run	Tensile strength < 1 min (MPa)	Tensile strength at 24 h, 65% RH (MPa)	Tensile strength at 24 h, 50% RH (MPa)
$A_2B_2C_3$	1.57	0.54	1.10
$A_2B_2C_2$	1.53	0.50	1.08

The validation results presented in Table 4 confirm that the actual performance of $A_2B_2C_2$ closely approximates the predicted values, with minor deviations attributable to experimental variability. This minor deviation suggests that under moderate humidity, the silane coupling agent contributes marginally beyond the level captured by the additive mean value model, likely through enhanced interfacial cross-linking that becomes disproportionately beneficial when the moisture flux is insufficient to challenge the physical barrier alone.

The divergence between the optimal formulations for initial and long-term tensile strengths reflects fundamentally distinct governing mechanisms that operate at different stages of the binder. The lower HEC dosage of 3% in the initial-strength-optimal formulation reduces the binder viscosity, thereby enhancing the wetting and penetration of the silicate binder into the interstices of the sand grain surfaces, which is the primary determinant of the instantaneous load-bearing capacity before significant siloxane condensation has occurred. Conversely, the elevated HEC dosages in the long-term-optimal formulations facilitate the formation of a continuous, entangled polymer film that physically

encapsulates the sand grains and creates a tortuous diffusion pathway for water molecules. This film-forming protection becomes the dominant mechanism under humid storage conditions.

Dosage exhibits consistently minor influence across all three responses, with the smallest range values in each case. This is consistent with its functional role as a dispersing agent that improves mixing homogeneity but does not directly participate in load-bearing network formation. The optimal TO dosage of 2% appears to provide adequate dispersing efficacy without introducing excessive surfactant residues.

The optimal KH550 content exhibits a pronounced humidity-dependent transition across the three-response metrics. This highlights that the silane coupling agent operates through a distinct mechanism from HEC and TO. While HEC and TO primarily influence the bulk properties and processability of the binder, KH550 functions at the molecular level by hydrolyzing its ethoxy groups to form silanol groups, which subsequently condense with the silicate oligomers and the surface hydroxyls of silica sand to generate covalent Si–O–Si bonds. This interfacial cross-linking is indispensable for both the rapid development of initial strength and the long-term preservation of network integrity against moisture-induced hydrolysis.

Under dry conditions, the silane functions primarily as an interfacial coupling agent; excessive loading promotes self-condensation and brittle polysiloxane formation, compromising cohesive strength. Under aggressive moisture attack, HEC film-forming dominates as the primary protective mechanism, while elevated KH550 undergoes excessive hydrolysis, destabilizing the Si–O–Si network and introducing defect sites. Under moderate humidity, the moisture flux is insufficient to compromise the intermediate HEC barrier, yet sufficient to permeate interfacial regions where KH550-mediated cross-linking becomes disproportionately beneficial. Thus, the divergence in optimal KH550 content reflects an environment-dependent strategy: moderate for dry adhesion, minimal for high-humidity barrier protection, and elevated for moderate-humidity interfacial reinforcement.

The comparative analysis across humidity conditions reveals a critical formulation strategy. For applications requiring high initial tensile strength, the formulation should prioritize reduced binder viscosity and enhanced interfacial wettability by employing a lower HEC dosage while maintaining an intermediate KH550 content to ensure adequate interfacial cross-linking without excessive silanol self-condensation. For extended storage stability under high-humidity conditions, the formulation should emphasize robust protective film formation through an elevated HEC dosage, coupled with a reduced KH550 level to prevent hydrolytic degradation of the interfacial Si–O–Si network. Under moderate-humidity environments, a balanced approach is optimal, with an intermediate HEC dosage and an elevated KH550 content to exploit the disproportionate benefit of interfacial cross-linking when the moisture flux is insufficient to challenge the physical barrier alone. In all scenarios, a consistent TO dosage of 2 wt% provides sufficient dispersing efficacy without introducing excessive surfactant residues.

3.4. The moisture resistance of sodium silicate-coated sand system

Due to the inherent hygroscopic nature of sodium silicate-coated sand, the specimens continuously absorb atmospheric moisture during storage, which progressively hydrolyzes the internal bonding bridges and leads to a decline in mechanical strength. Macroscopically, this degradation manifests as a perceptible softening of the specimen upon handling and severe surface sand shedding. These concurrent phenomena render precise gravimetric measurement of water absorption highly problematic, as the mass loss induced by surface sand detachment cannot be reliably distinguished from the mass gain associated with moisture uptake. Consequently, the water absorption rate calculated from the mass difference before and after exposure lacks the requisite rigor for quantitative assessment. Considering these limitations, the 24-hour strength retention rate was adopted in this study as the definitive criterion for evaluating the moisture resistance of the modified sodium silicate-coated sand. This metric directly reflects the structural integrity of the bonding bridges after moisture exposure and is independent of the confounding effects associated with surface erosion or mass fluctuation, thereby providing a more robust and reproducible measure of hydrolytic durability. The relevant strength retention data are presented in Fig. 6. The range analysis of the orthogonal array design for the 24 h strength retention rate reveals distinct factor hierarchies and environment-dependent optimal formulations, as summarized in Table 5 and Table 6.

Table 5 Orthogonal experimental results for strength retention rate

Run	Factor A (HEC, wt%)	Factor B (TO, wt%)	Factor C (KH550, wt%)	Strength retention rate at 24 h, 65% RH (%)	Strength retention rate at 24 h, 50% RH (%)
1	1(3)	1(1)	1(5)	38.51	47.20
2	1(3)	2(2)	2(10)	36.14	54.66
3	1(3)	3(5)	3(15)	38.04	43.98
4	2(4)	1(1)	2(10)	30.72	67.97
5	2(4)	2(2)	3(15)	34.39	70.06
6	2(4)	3(5)	1(5)	41.91	69.85
7	3(5)	1(1)	3(15)	48.55	64.49
8	3(5)	2(2)	1(5)	47.22	59.72
9	3(5)	3(5)	2(10)	39.61	54.97

Table 6 Analysis of orthogonal experimental results for strength retention rate

Response	Factor	k_1	k_2	k_3	R	Rank
Strength retention rate at 24 h, 65% RH (%)	A (HEC)	37.56	35.67	45.13	9.46	1
	B(TO)	39.26	39.25	39.85	0.60	3
	C(KH550)	42.55	35.49	40.33	7.06	2
Strength retention rate at 24 h, 50% RH (%)	A (HEC)	48.61	69.29	59.73	20.68	1
	B(TO)	59.89	61.48	56.27	5.21	2
	C(KH550)	58.92	59.20	59.51	0.59	3

At 65% RH, the influence ranking follows the order HEC > KH550 > TO. The theoretically predicted optimum is $A_3B_3C_1$. The experimentally achieved maximum of 48.55 MPa occurs in Run 7 ($A_3B_1C_3$). Based on the primary orthogonal experimental results, the deviation between the theoretically optimal formulation and the actual maximum for the 24-hour strength retention rate at 65% RH warrants targeted comparative analysis. Six replicate tests were conducted for each experimental run, and the average of the six measurements was reported as the result. The results of the validation experiments are presented in Table 7.

Table 7 Validation test for strength retention rate

Run	Strength retention rate at 24 h, 65% RH (%)	Strength retention rate at 24 h, 50% RH (%)
$A_3B_3C_1$	48.62	58.21
$A_3B_1C_3$	49.23	64.44

The validation experiments presented in **Table 7** reveal that the theoretically predicted optimum $A_3B_3C_1$ is marginally outperformed by $A_3B_1C_3$ under both humidity conditions, with strength retention rates of 49.23 MPa versus 48.62 MPa at 65% RH and 64.44 MPa versus 58.21 MPa at 50% RH. This deviation can be attributed to the inherent limitations of the additive mean-value model employed in the range analysis, which assumes factor independence and thereby neglects potential interaction effects. Specifically, the orthogonal array design yields a negligible range for TO (R = 0.60 MPa at 65% RH), indicating that the selection of B_3 over B_1 lacks statistical significance and is susceptible to experimental variability. Under the dominant physical barrier conferred by the maximum HEC dosage, the reduction of TO from 5% to 1% diminishes surfactant residues at the interface, thereby facilitating unimpeded access of silanol groups to the sand grain surface hydroxyls and silicate oligomers. This synergistic enhancement enables the elevated KH550 content to exert a disproportionately beneficial cross-linking effect that transcends the additive model prediction. Furthermore, the absolute deviation between the theoretical and validated maxima falls within the expected experimental error margin for a design with three replicates per level. Consequently, both $A_3B_3C_1$ and $A_3B_1C_3$ can be considered near-optimal formulations, with the final selection dictated by practical considerations such as raw material cost and processing tolerance.

At 50% RH, the influence of hierarchy shifts to HEC > TO > KH550. The theoretically optimal combination $A_2B_2C_3$ achieves exact concordance with the experimental maximum of 70.06 MPa in Run 5, validating the reliability of the additive model under moderate humidity. Notably, HEC remains the primary determinant across both environments, yet its optimal dosage decreases from the highest level under high humidity to an intermediate level under moderate humidity. Conversely, the KH550 exhibits an inverse trend: its optimal content shifts from the minimum level at 65% RH to the maximum level at 50% RH. This humidity-dependent inversion underscores that under aggressive moisture flux, excessive silane promotes hydrolytic degradation of interfacial Si–O–Si bonds, whereas under moderate humidity, enhanced interfacial cross-linking becomes disproportionately beneficial. Throughout both regimes, TO exerts a consistently minor influence, confirming its auxiliary role as a dispersing agent.

All formulations exhibit substantially higher retention rates at 50% RH compared to 65% RH, with differential values ranging from 5.93% to 37.25%. This consistent humidity dependency confirms that moisture ingress is the primary driver of hydrolytic degradation in the silicate binder network, and that the protective efficacy of the organic modifiers is strongly modulated by the ambient water vapor pressure. This underscores the critical role of the HEC film-forming function under aggressive moisture conditions, where a dense, continuous polymer network is required to physically shield the underlying siloxane bonds from hydrolytic attack. KH550 at its high-level yields superior retention, while TO exhibits minimal effect, indicating that dispersing agent dosage is inconsequential to moisture resistance at high humidity. Under moderate humidity, excessive film thickness may introduce interfacial stress or reduce binder cohesion, while insufficient coverage leaves the network inadequately protected. The diminished influence of KH550 at 50% RH indicates that the reduced moisture flux relaxes the demand for dense siloxane cross-linking, and that the physical barrier mechanism of HEC becomes the dominant protective pathway.

Nevertheless, the hydroxyl-rich structure of HEC presents a paradoxical effect on the moisture resistance of the coated sand. On one hand, these hydroxyl groups are essential for film-forming and interfacial adhesion; on the other hand, their intrinsic hydrophilicity renders the binder susceptible to moisture absorption. The experimental data reveals a non-monotonic relationship between HEC dosage and strength retention.

The optimal HEC dosage of 5% achieves an optimal balance between film thickness and binder viscosity. Insufficient HEC coverage leaves the silicate network inadequately encapsulated, failing to establish a continuous protective film and exposing the underlying Si-O-Si bonds to direct moisture attack. Under such conditions, the physical barrier effect is markedly weakened, allowing water molecules to readily penetrate the binder-sand interface and hydrolyze the siloxane cross-links. Further increasing the HEC dosage beyond 5% will lead to a decline in moisture resistance. Excessive hydroxyl groups would absorb atmospheric moisture through hydrogen bonding and cause the HEC film to swell. Such swelling can induce microcracking within the film, creating preferential pathways for water ingress and ultimately weakening the interfacial bonding. TO exhibits minimal direct influence on mechanical properties, consistent with its role as a dispersing agent that improves interfacial compatibility during mixing.

In summary, the orthogonal experimental design and subsequent validation trials collectively establish a mechanistic framework for tailoring silicate-based sand binder formulations to specific service environments. The divergence in optimal additive dosages across humidity regimes reflects a fundamental transition in the governing protection mechanism: under aggressive moisture attack, the HEC film-forming function dominates as the primary barrier, necessitating its maximum dosage while suppressing KH550 to prevent hydrolytic degradation; under moderate humidity, a balanced approach is optimal, with intermediate HEC and elevated KH550 synergistically enhancing both physical shielding and interfacial cross-linking. The consistently minor influence of TO underscores its auxiliary role in processability rather than performance. These findings provide a rational, data-driven basis for formulating moisture-resistant silicate binders, with the final selection among near-optimal combinations dictated by practical constraints, including raw material cost, processing tolerance, and the anticipated storage humidity profile.

3.5. The collapsibility of sodium silicate-coated sand system

Collapsibility is a critical service performance of sodium silicate-coated sand. After casting and solidification of the casting, the high-temperature thermal effect destroys the internal binder bridging structure of the coated sand, resulting in a sharp decline in the strength of the sand mould. The spent sand can be easily crushed and detached from the surface and inner cavity of the casting, which facilitates subsequent cleaning operations. In contrast, coated sand with poor collapsibility maintains high residual strength after casting, requiring manual chiseling and forced crushing for mould removal. This not only increases the cleaning cost and production workload but also easily causes surface damage and dimensional defects to the castings. As shown in Fig. 7(a) and Fig. 7(b), the collapsibility of sodium silicate-coated sand is quantified as the mass ratio of sand passing through a 10-mesh sieve to the residual sand retained on the sieve, with higher values indicating superior shakeout performance, which can objectively reflect the high-temperature collapse behavior of different modified binder systems. Fig. 7(c) presents the collapsibility of the modified sodium silicate-coated sand after calcination at 400 °C for 5 min, measured under two storage humidity conditions (65% and 50% RH) prior to thermal treatment. Tables 8 and 9 present the orthogonal experimental results and the corresponding analysis for collapsibility.

Table 8 Orthogonal experimental results for collapsibility

Run	Factor A (HEC, wt%)	Factor B (TO, wt%)	Factor C (KH550, wt%)	Collapsibility at 24 h, 65% RH (%)	Collapsibility at 24 h, 50% RH (%)
1	1(3)	1(1)	1(5)	17.35	39.27
2	1(3)	2(2)	2(10)	23.39	27.59
3	1(3)	3(5)	3(15)	23.34	26.70
4	2(4)	1(1)	2(10)	28.66	28.72
5	2(4)	2(2)	3(15)	21.81	30.14
6	2(4)	3(5)	1(5)	34.35	47.73
7	3(5)	1(1)	3(15)	25.57	32.16
8	3(5)	2(2)	1(5)	47.16	72.69
9	3(5)	3(5)	2(10)	29.97	50.31

Table 9 Analysis of orthogonal experimental results for collapsibility

Response	**Factor**	**k_1**	**k2**	**k3**	**R**	**Rank**
Collapsibility at 24 h, 65% RH (%)	A (HEC)	21.36	28.27	34.23	12.87	1
	B(TO)	23.86	30.79	29.22	6.93	3
	C(KH550)	32.95	27.34	23.57	9.38	2
Collapsibility at 24 h, 50% RH (%)	A (HEC)	31.19	35.53	51.72	20.53	2
	B(TO)	33.38	43.47	41.58	10.09	3
	C(KH550)	53.23	35.54	29.67	23.56	1

At 65% RH, the influence ranking follows the order HEC > KH550 > TO. The theoretically predicted optimum $A_3B_2C_1$ achieves exact concordance with the experimental maximum of 47.16% in Run 8, validating the reliability of the additive model. HEC emerges as the primary positive driver, with its elevated dosage promoting the formation of a thick organic film that undergoes thermal decomposition at 400 °C to generate porous channels within the binder matrix, thereby facilitating the disintegration of the rigid silicate ceramic phase upon mechanical agitation. Conversely, KH550 exhibits a pronounced negative correlation (K_1 = 32.95% > K_2 = 27.34% > K_3 = 23.57%), indicating that elevated silane content enhances interfacial Si–O–Si ceramization, which strengthens the high-temperature ceramic bonding and impedes sand grain detachment. At 50% RH, the influence of hierarchy shifts to KH550 > HEC > TO. The theoretically optimal combination $A_3B_2C_1$ again achieves exact concordance with the experimental maximum of 72.69% in Run 8. Notably, KH550 assumes dominant negative control under moderate

humidity, with its K_1 value (53.23%) nearly doubling K_3 (29.67%). This amplified sensitivity underscores that the reduced moisture flux during storage preserves a more intact siloxane cross-linked network, which subsequently undergoes extensive high temperature ceramization, thereby magnifying the detrimental effect of elevated KH550 on post-casting shakeout.

All formulations exhibit substantially higher collapsibility at 50% RH compared to 65% RH, with differential values ranging from 0.66% to 25.53%. This consistent trend indicates that storage humidity influences the subsequent high-temperature breakdown behavior, likely through moisture-induced modifications to the binder network architecture that alter its thermal response.

The consistent attainment of the actual maximum by $A_3B_2C_1$ across both humidity regimes establishes this formulation as a robust, environment-tolerant choice for optimizing collapsibility. The divergence in factor dominance—HEC-controlled at 65% RH versus KH550-controlled at 50% RH reflects a mechanistic transition in the governing degradation pathway: under aggressive moisture attack, the physical barrier function of HEC governs the preservation of binder architecture and thus the residual organic fraction available for thermal porosification, whereas under moderate humidity, the extent of interfacial siloxane condensation becomes the primary determinant of high-temperature ceramic bonding strength. In both regimes, TO exerts a secondary influence, with an intermediate dosage of 2% providing adequate dispersing efficacy without introducing excessive surfactant residues that could reinforce the binder network.

The humidity sensitivity of collapsibility varies markedly across formulations. Runs 8 and 1, both featuring low KH550 at 5%, exhibit the largest differentials of 25.53% and 21.92%, suggesting that formulations with minimal interfacial ceramization are more susceptible to humidity-induced structural modifications that subsequently influence their thermal breakdown. In contrast, runs 4 and 3, with intermediate-to-elevated KH550 at 10–15%, display minimal differentials of 0.06% and 3.36%, indicating that dense siloxane cross-linked networks maintain more consistent decomposition behavior at elevated temperatures regardless of pre-storage humidity. Notably, run 6, with an intermediate HEC at 4% and a low KH550 at 5%, exhibits a substantial differential of 13.38%, underscoring that the combination of moderate film thickness with minimal interfacial ceramization creates a humidity-responsive system in which moisture ingress during storage significantly alters the thermal decomposition pathway.

In summary, the collapsibility data demonstrates that HEC dosage is the primary positive driver at 65% RH, while KH550 dosage assumes dominant negative control at 50% RH, reflecting its critical role in governing the extent of high temperature ceramization. KH550 exhibits a consistently negative correlation across both humidity conditions, with low KH550 yielding superior shakeout performance by minimizing the formation of rigid Si–O–Si ceramic bonds. The dosage exerts a secondary influence, with an intermediate level of 2% providing optimal dispersing efficacy without introducing excessive surfactant residues. For applications prioritizing post-casting shakeout efficiency, the formulation $A_3B_2C_1$ is recommended across both humidity regimes, achieving 47.16% at 65% RH and 72.69% at 50% RH. This formulation establishes a robust balance between film-forming-induced porosification and

minimal interfacial ceramization. Conversely, applications demanding maximum strength retention must accept compromised collapsibility through elevated KH550 content, which promotes interfacial cross-linking and ceramization. This fundamental trade-off between moisture resistance and thermal disintegration underscores the necessity of application-specific formulation optimization in multi-component modified sodium silicate binder systems.

4. Conclusion

In order to improve the moisture resistance and collapsibility of the sodium silicate coated sand solidification system, HEC organic polymer was introduced to improve the collapsibility, tung oil long-chain was introduced to improve the moisture resistance, and KH550 was introduced to improve the interface characteristics between organic compounds and sand. The single and multiple factors affecting three types of organic compounds were studied, and the best method that combines collapsibility and moisture resistance was reached. The divergence between these optimal formulations for initial strength, high-humidity storage, moderate-humidity storage, and post-casting shakeout underscores the necessity of tailoring binder compositions to specific foundry environments, establishing a rational, evidence-based framework for the design of environmentally friendly sodium silicate binders as viable alternatives to phenolic resin systems. Nevertheless, the L9(3^3) orthogonal design with only nine runs and three levels per factor provides limited resolution for capturing non-linear effects and modifier interactions. Future studies should employ response surface methodology with finer dosage gradients, expand the environmental parameter space, and validate formulations through full-scale casting trials.

Declarations

Author Contribution

Tengxiao Luo: data curation, methodology, validation, wrote the main manuscript text.Junhua Zhang: conceptualization, funding acquisition, investigation, reviewed the manuscript

Acknowledgement

This work was supported by the National Key Laboratory of Advanced Polymer Materials and the Analytical & Testing Center of Sichuan University.

Funding Declaration

The authors did not receive support from any organization for the submitted work. The authors declare that they have no known competing financial interests or personal relationships that could have appeared to influence the work reported in this paper.

References

1. F. Ettemeyer, M. Schweinefuß, P. Lechner, J. Stahl, T. Greß, J. Kaindl, L. Durach, W. Volk, D. Günther, J. Mater. Process. Technol. 296, 117201 (2021). https://doi.org/10.1016/j.jmatprotec.2021.117201
2. Y. Xu, G. Li, W. Jiang, J. Zhan, Y. Yu, Z. Fan, J. Mater. Res. Technol. 19, 4063–4075 (2022). https://doi.org/10.1016/j.jmrt.2022.06.148
3. S. Żymankowska-Kumon, Arch. Foundry Eng. 18, 83–86 (2018). https://doi.org/10.24425/afe.2018.125173
4. A. Kmita, C. Fischer, K. Hodor, M. Holtzer, A. Roczniak, Arab. J. Chem. 11, 380–387 (2018). https://doi.org/10.1016/j.arabjc.2016.11.003
5. M. Holtzer, R. Dańko, S. Piasny, M. Kubecki, D. Drożyński, A. Roczniak, M. Skrzyński, A. Kmita, Materials 14, 2581 (2021). https://doi.org/10.3390/ma14102581
6. M. Holtzer, R. Dańko, A. Kmita, D. Drożyński, M. Kubecki, M. Skrzyński, A. Roczniak, Materials 13, 4395 (2020). https://doi.org/10.3390/ma13194395
7. C.E. Bates, L.D. Scheel, Am. Ind. Hyg. Assoc. J. 35, 452–462 (1974). https://doi.org/10.1080/0002889748507059
8. C. Alias, F. Cioli, A. Abbà, D. Feretti, S. Sorlini, Integr. Environ. Assess. Manag. 20, 2294–2311 (2024). https://doi.org/10.1002/ieam.4983
9. Anwar, N., Major-Gabryś, K., Jalava, K. et al. Effect of Additives on Heat Hardened Inorganic Solid Foundry Binder. Inter Metalcast 19, 129–144 (2024). https://doi.org/10.1007/s40962-024-01277-w
10. A. Kmita, A. Roczniak, Arch. Foundry Eng. 17, 93–98 (2017). https://doi.org/10.1515/afe-2017-0017
11. E.-H. Kim, W.-R. Lee, Y.-G. Jung, C.-S. Lee, Mater. Chem. Phys. 126, 344–351 (2011). https://doi.org/10.1016/j.matchemphys.2010.11.015
12. S. Lucas, M.T. Tognonvi, J.L. Gelet, J. Soro, S. Rossignol, J. Non-Cryst. Solids 357, 1310–1318 (2011). https://doi.org/10.1016/j.jnoncrysol.2010.12.016
13. I. Izdebska-Szanda, A. Baliński, M. Angrecki, Arch. Foundry Eng. 12, 35–40 (2012). https://doi.org/10.2478/v10266-012-0032-y
14. L. Song, X. Du, W. Cao, J. Zhao, G. Song, Y. Sun, X. Ma, R. Tao, Silicon 16, 73–81 (2024). https://doi.org/10.1007/s12633-023-02657-3
15. Zaretskiy, L. Modified Silicate Binders New Developments and Applications. Inter Metalcast 10, 88–99 (2015). https://doi.org/10.1007/s40962-015-0005-3
16. M. Stachowicz, K. Granat, Arch. Metall. Mater. 59, 757–760 (2014). https://doi.org/10.2478/amm-2014-0127

17. L. Song, W. Liu, F. Xin, Y. Li, Int. J. Adhes. Adhes. 106, 102820 (2021). https://doi.org/10.1016/j.ijadhadh.2021.102820
18. M. Yang, J. Su, Y. Zheng, C. Fang, W. Lei, L. Li, Polymers 15, 3525 (2023). https://doi.org/10.3390/polym15173525
19. Anwar, N., Jalava, K. et al. Experimental Study of Inorganic Foundry Sand Binders for Mold and Cast Quality. Inter Metalcast 17, 1697–1714 (2022). https://doi.org/10.1007/s40962-022-00897-4
20. Zhao, K., Liu, W., Song, L. et al. Research on the Relationship between Sodium Bicarbonate Content and "Over-gassing" in the Core Making Process of CO_2 Hardening Sodium Silicate Sand. Inter Metalcast 16, 2144–2149 (2022). https://doi.org/10.1007/s40962-022-00805-w
21. Song, L., Liu, W., Xin, F. et al. "Materials Studio" Simulation Study of the Adsorption and Polymerization Mechanism of Sodium Silicate on Active Silica Surface at Different Temperatures. Inter Metalcast 15, 1091–1098 (2020). https://doi.org/10.1007/s40962-019-00405-1
22. Xin, F., Liu, W., Song, L. et al. Research of Compound Additives on Moisture Resistance of Sand Cores Bonded by Sodium Silicate. Inter Metalcast 17, 753–760 (2022). https://doi.org/10.1007/s40962-022-00805-w
23. O, G.H., Choe, K.C. et al. Effect of Sodium Phosphate on the Properties of Sodium Silicate and Collapsibility of Sodium Silicate Sand. Inter Metalcast 17, 297–304 (2022). https://doi.org/10.1007/s40962-021-00716-2
24. Zaretskiy, L. Microsilica in Sodium Silicate Bonded Sands. Inter Metalcast 13, 58–73 (2018). https://doi.org/10.1007/s40962-018-0247-y
25. Ünlü, N., Odabaş, A. Development and Evaluation of a New Eco-friendly Sodium Silicate-Based Binder System. Inter Metalcast 12, 765–771 (2018). https://doi.org/10.1007/s40962-018-0210-y
26. X. Gao, Q. Zhou, Y. Wang, T. Qi, L. Shen, G. Liu, Z. Peng, X. Li, Process Saf. Environ. Prot. 171, 396–404 (2023). https://doi.org/10.1016/j.psep.2023.01.022
27. S. Onutai, T. Osugi, T. Sone, Materials 16, 3985 (2023). https://doi.org/10.3390/ma16030985
28. G.D. Poggetto, C. Leonelli, A. Spinella, J. Mater. Sci. 59, 16963–16980 (2024). https://doi.org/10.1007/s10853-024-09869-x
29. B. Wei, Q. Chang, C. Bao, L. Dai, G. Zhang, F. Wu, Colloids Surf. A 434, 276–280 (2013). https://doi.org/10.1016/j.colsurfa.2013.05.069
30. B. Qiao, T.-J. Wang, H. Gao, Y. Jin, Appl. Surf. Sci. 351, 646–654 (2015). https://doi.org/10.1016/j.apsusc.2015.05.174

Figures

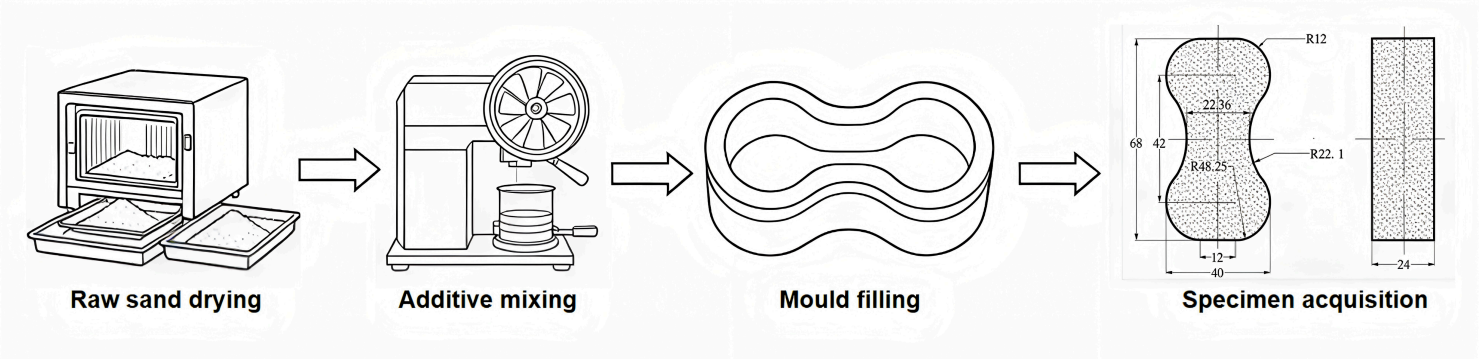


Figure 1

Preparation process of modified sodium silicate-coated sand and specimen molding

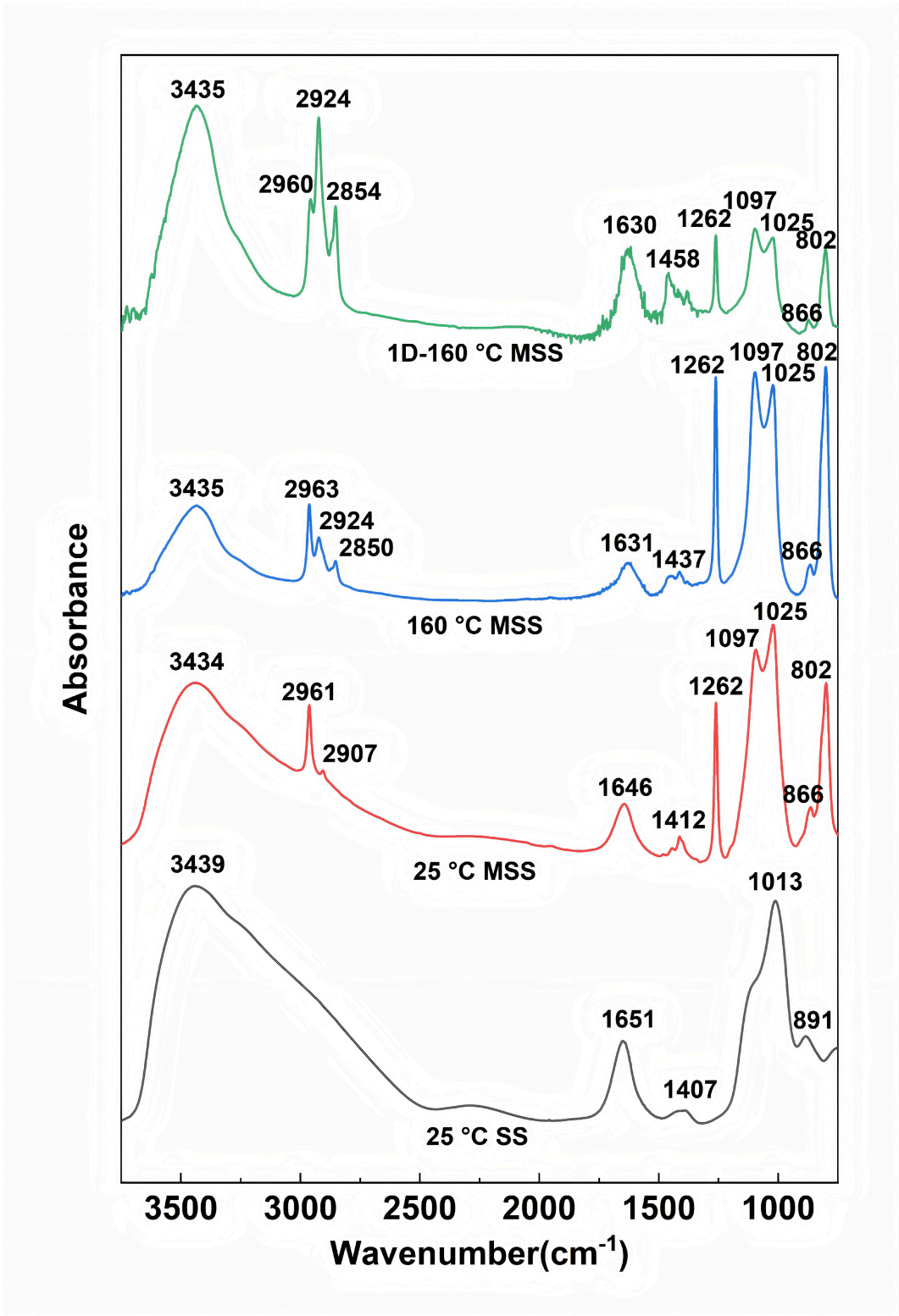


Figure 2

FTIR spectra of sodium silicate systems under different conditions: (black) pure sodium silicate (SS) system at 25 ℃; (red) modified sodium silicate (MSS) system at 25 ℃; (blue) modified sodium silicate system at 160 ℃; (green) modified sodium silicate system at 160 ℃ after one-day storage

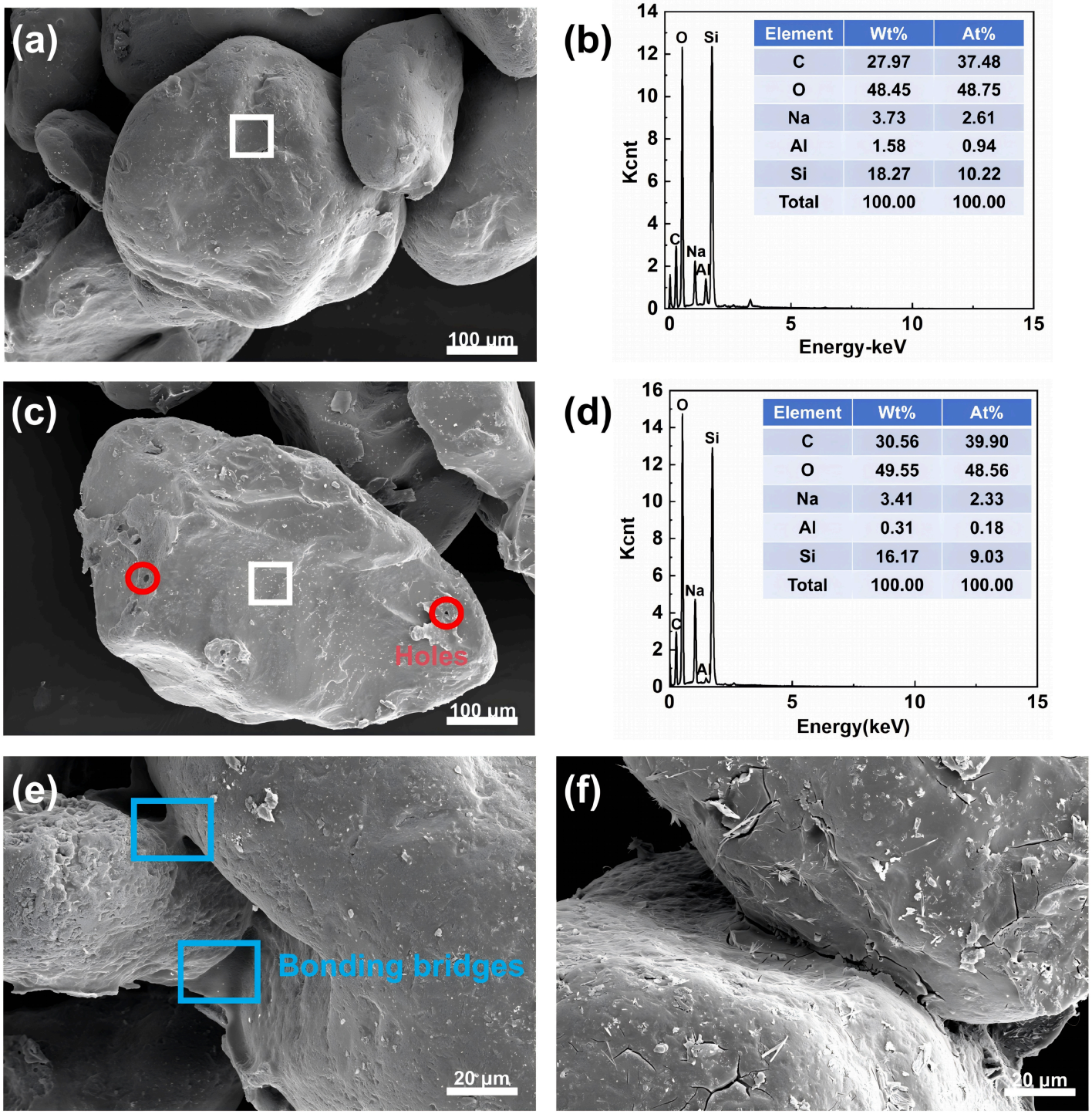


Figure 3

SEM micrographs and EDS analyses of sodium silicate-coated sand samples: (a) SEM image of the modified sodium silicatesystem; (b) EDS spectrum of the local area marked by the white square in (a); (c) SEM image of the unmodified sodium silicate system; (d) EDS spectrum of the local area marked by the white square in (c); (e) SEM image of the modified sodium silicate system after one-day storage; (f) SEM image of the unmodified sodium silicate system after one-day storage

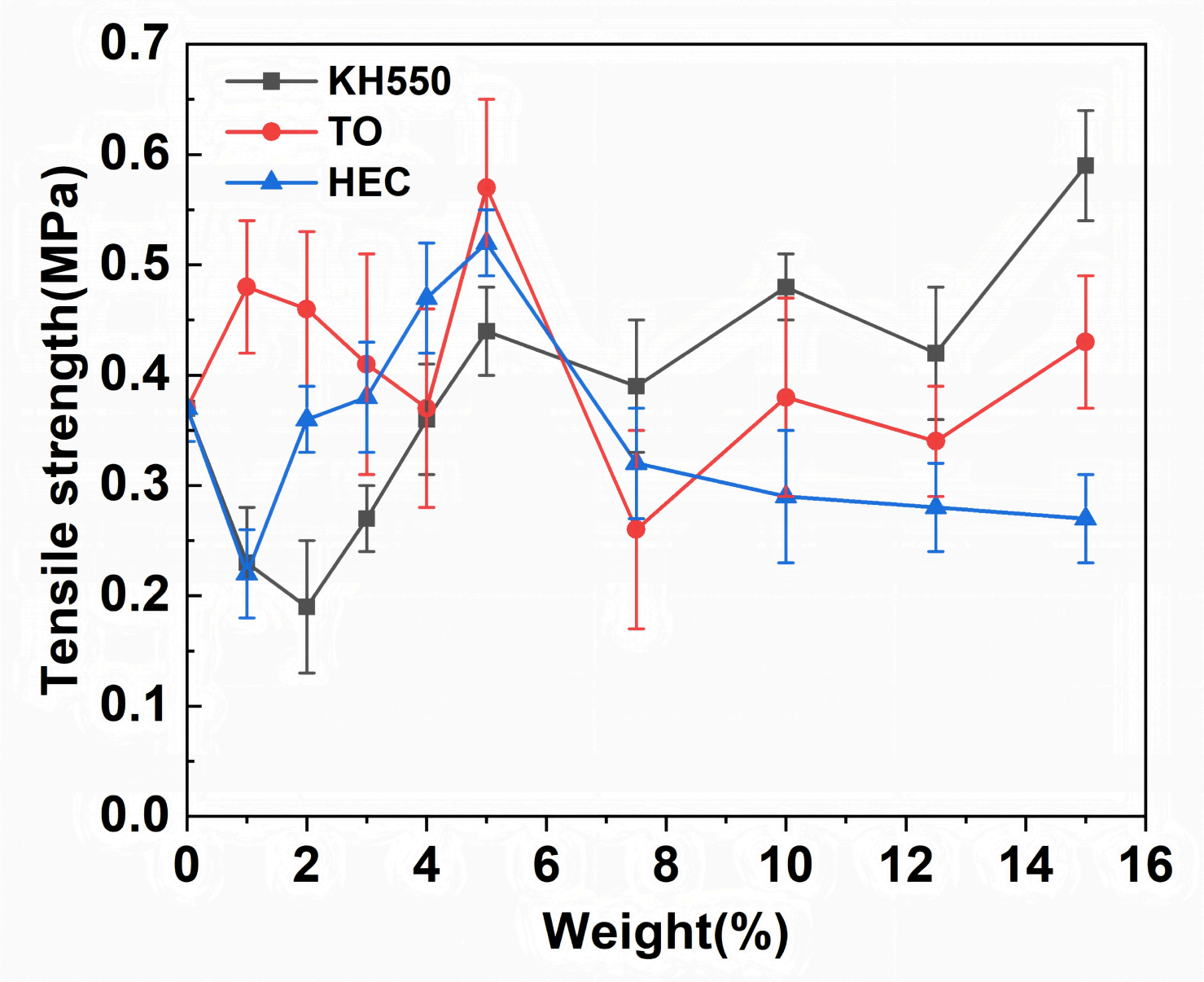


Figure 4

Effect of individual modifier dosage on the 24-hour residual tensile strength of modified sodium silicate-coated sand

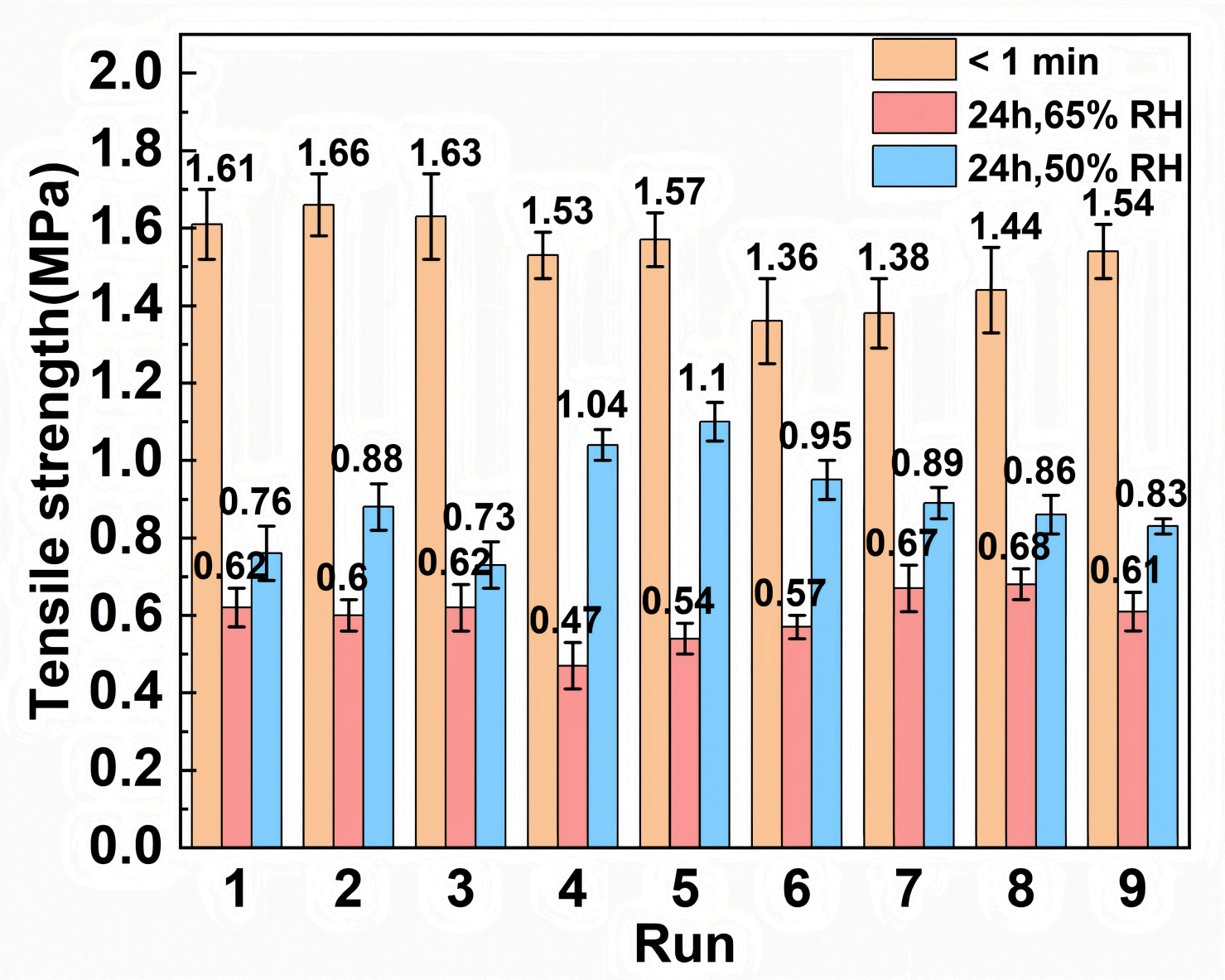


Figure 5

Tensile strength of modified sodium silicate-coated sand under three conditions: initial (< 1 min), and after 24 h at 65% and 50% RH

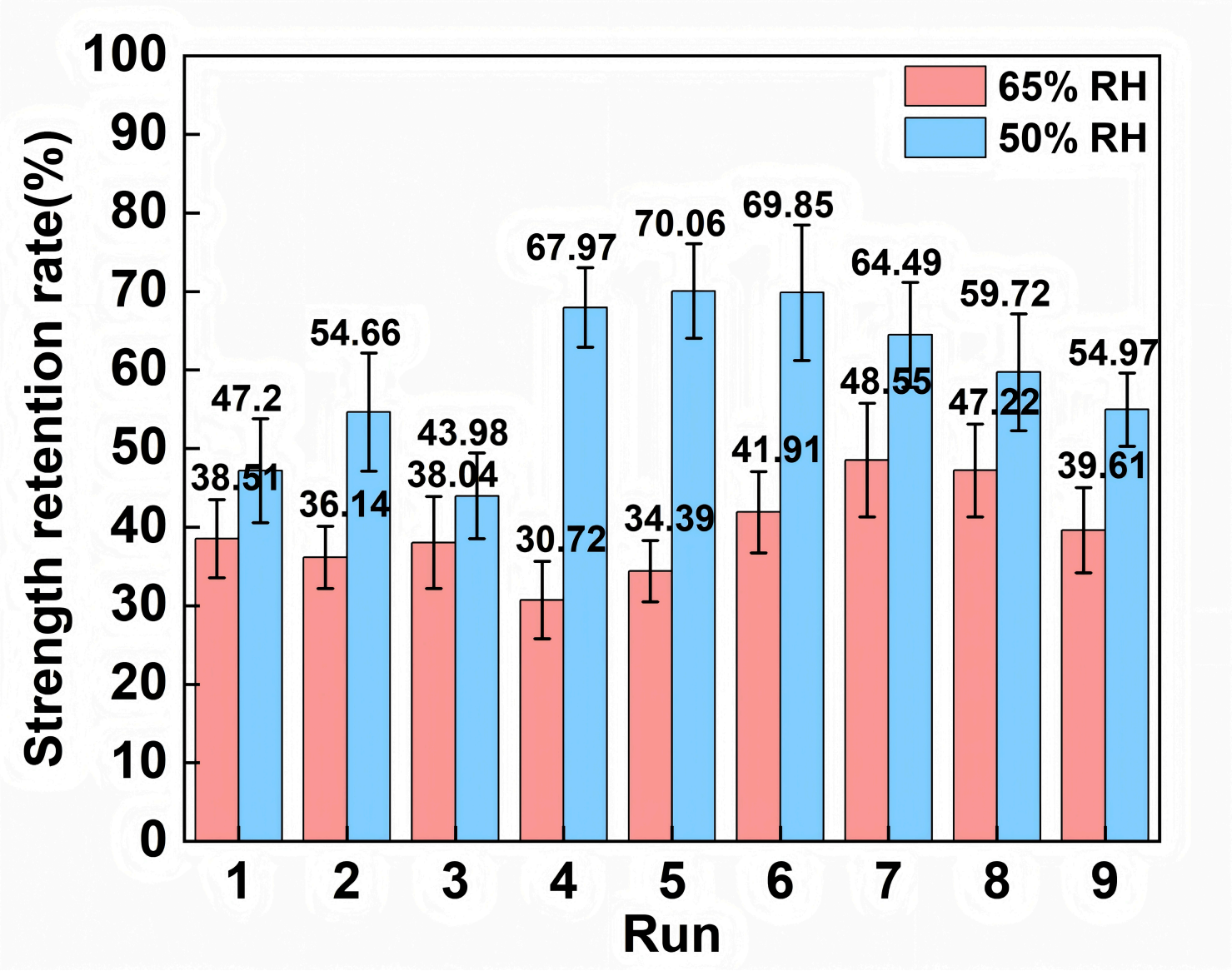


Figure 6

Strength retention rate of modified sodium silicate-coated sand after 24 h at 65% and 50% RH

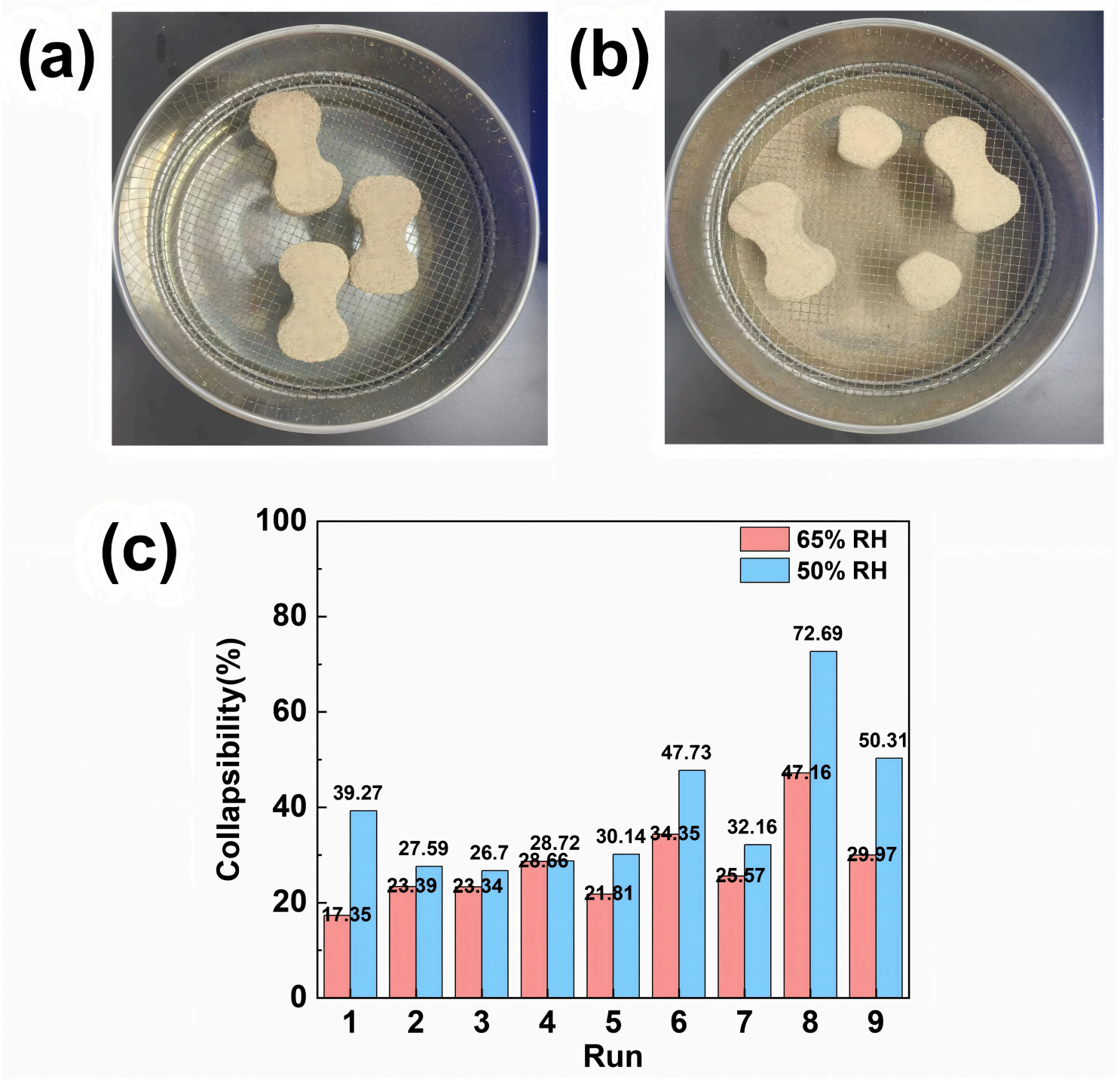


Figure 7

Collapsibility of modified sodium silicate-coated sand: (a, b) calcined specimens on a 10-mesh vibrating sieve; (c) collapsibility after 24 h storage at 65% and 50% 50% RH